Direct Measurement of Electron Transfer Distance Decay Constants of Single Redox Proteins by Electrochemical Tunneling Spectroscopy

Juan M. Artés,[†,‡] Ismael Díez-Pérez,[†] Fausto Sanz,[†,‡,§] and Pau Gorostiza[†,§,⊥,*]

[†]Institute for Bioengineering of Catalonia (IBEC), 15-21 Baldiri Reixac, 08028 Barcelona, Spain, [‡]Physical Chemistry Department, University of Barcelona (UB), 1-11 Martí i Franquès, 08028 Barcelona, Spain, [§]Networking Research Center on Bioengineering, Biomaterials and Nanomedicine (CIBER-BBN), and [⊥]Institució Catalana de Recerca i Estudis Avançats (ICREA)

ABSTRACT We present a method to measure directly and at the single-molecule level the distance decay constant that characterizes the rate of electron transfer (ET) in redox proteins. Using an electrochemical tunneling microscope under bipotentiostatic control, we obtained current−distance spectroscopic recordings of individual redox proteins confined within a nanometric tunneling gap at a well-defined molecular orientation. The tunneling current decays exponentially, and the corresponding decay constant (β) strongly supports a two-step tunneling ET mechanism. Statistical analysis of decay constant measurements reveals differences between the reduced and oxidized states that may be relevant to the control of ET rates in enzymes and biological electron transport chains.

KEYWORDS: long-range electron transfer (LRET) · distance decay constant · single-molecule electrochemistry · redox enzyme · metalloprotein · blue copper protein · azurin · electrochemical scanning tunneling microscopy and spectroscopy · nanoelectrodes · Debye length · electrochemical charge screening

Electron transfer (ET) reactions are essential in many chemical and biological processes,[1] such as cellular respiration and photosynthesis. The study of ET is important not only to understand how enzymes work[2] but to put forward technological applications in biosensing[3] and molecular electronics.[4,5] Methods to measure ET at the single-molecule level are expected both to resolve temporal variations in enzyme activity that can be correlated with conformational changes[6] and to allow the ultimate miniaturization of nanodevices. The blue copper protein azurin (Az) acts as a soluble electron carrier in the respiratory chain of bacteria and constitutes a convenient model system to investigate ET that has been the object of many studies.[7−9] *Pseudomonas aeruginosa* Az is a globular protein that contains a Cu ion coordinated by protein residues, which makes the protein capable of accepting and transporting electrons by switching its redox state ($Cu^{I/II}$). The rate k_{ET} of nonadiabatic ET at a fixed distance between a donor (A) and an acceptor (B) is described by semiclassical Marcus theory using eq 1:[1,10]

$$k_{ET} = \sqrt{\frac{4\pi^3}{h^2\lambda k_B T}}\, H_{AB}^2 \exp\left\{-\frac{(\Delta G+\lambda)^2}{4\lambda k_B T}\right\} \quad (1)$$

where k_{ET} depends on the driving force ($\Delta G°$) of the ET reaction, the reorganization energy (λ), the temperature (T), and the electronic coupling between A and B (H_{AB}), and the k_B and h are the Boltzmann and Planck constants, respectively. The coupling H_{AB} and thus the rate of ET are expected to have an exponential dependence on the donor−acceptor distance (d_{AB}). The key parameter in this relationship is the distance decay constant β, which is characteristic of the molecule involved in ET and the transfer mechanism:

$$k_{ET} \propto \exp(-\beta d_{AB}) \quad (2)$$

It has long been discussed how the rate of ET to and from a redox center is influenced by the protein matrix surrounding it in redox proteins.[10,11] Recent advances have demonstrated that amino acids of the protein fine-tune its redox potential[12,13] and act as semiconductor relay elements to facilitate the transfer,[8] thus confirming the tunneling pathway model predicted by calculations.[14] However, tunneling decay constants are

* Address correspondence to pau@icrea.cat.

Received for review November 28, 2010 and accepted February 15, 2011.

Published online February 25, 2011
10.1021/nn103236e

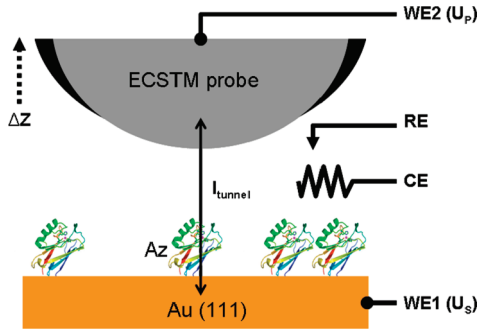

Figure 1. Experimental setup for ECSTM imaging and current−distance spectroscopy studies of azurin under bipotentiostatic control. Azurin proteins are bound by means of native cysteines to an atomically flat Au ⟨111⟩ surface, which constitutes one of the working electrodes of the bipotentiostatic control system (WE1, electrochemical potential of the sample noted U_S in the text). The ECSTM probe is a sharp Pt−Ir needle coated with an electrical insulator (black) that exposes only the tip apex and constitutes the second working electrode (WE2, electrochemical potential noted U_P in the text). RE denotes the reference electrode in solution and CE the auxiliary or counter electrode (see Methods for details). Tunneling current measurements between WE1 and WE2 allow performing ECSTM imaging and current−distance (I−z) spectroscopic measurements at single protein resolution.

usually obtained indirectly by the determination of macroscopic rate constants from optical and infrared spectroscopy, and then applying the semiclassical Marcus theory[1] in order to calculate the kinetic, thermodynamic, and electronic parameters of the process. Experimental determination of a distance decay constant (β) in a protein was achieved by measuring the ET rate between $Cu^{I/II}$ center of the blue copper protein azurin and redox probes ($Ru^{II/III}$) attached to histidine residues mutated at different points on the surface of the protein. Rates were then plotted in a logarithmic axis *versus* the linear distance between the Cu center and each mutated residue.[7] This method yielded a distance decay factor $\beta = 11$ nm^{-1}, in agreement with calculations[14] and electrochemical measurements.[15,16] Together, these results established superexchange tunneling as the mechanism of intraprotein ET in azurin.[10] Current−distance recordings by ECTS can be compared to electrochemical measurements with redox probes introduced at different distances along a well-defined axis of the protein. The tip of an electrochemical scanning tunneling microscope (ECSTM) constitutes an electrochemical probe whose Fermi energy can be adjusted at any desired value within the solvent window and whose position with respect to an individual protein can be fixed or scanned along any direction with subnanometer accuracy,[17] giving rise to single-molecule measurements. Indeed, ET has been studied at the single-molecule level by STM,[18] ECSTM,[15] by conductive probe atomic force microscopy,[19] and using molecular junctions.[20,21] It was first observed by ECSTM that Fe-protoporphyrin molecules on graphite display a resonant-like behavior of the tunneling ET,[22] a feature that has been later reported for other molecules, including proteins.[15,23]

Here we report current−distance measurements using an ECSTM under bipotentiostatic control in order to determine directly and at single-molecule level the current−distance decay constant (β) for intermolecular ET with azurin at a fixed orientation and as a function of its redox state. ECSTM probes were insulated except at the apex in order to minimize faradaic current,[24] and individual proteins were further confined within the tunneling gap between the probe and an atomically flat gold surface (Figure 1). Our measurements confirm the two-step ET tunneling mechanism with values of β in agreement with previous reports[15,25] and with theoretical predictions for multistep intermolecular ET.[26] In addition, β is found to depend significantly on the redox state of the protein, which points out the key role of the Cu redox center in the ET mechanism as previously suggested.[15,23] Similarly, the presence of oxidizable residues along the ET pathway has been demonstrated to directly participate in the ET process.[8] At short probe−protein distances, incomplete charge screening effects are also observed that affect imaging and spectroscopic measurements.

RESULTS AND DISCUSSION

ECSTM Imaging. Imaging of azurin on gold by ECSTM under bipotentiostatic control (see Figure 1 and Supporting Information Figure S1) shows nanometric particles of uniform height evenly distributed on the surface that correspond to individual proteins or clusters.[25] As in previous studies, we observed changes in the apparent height of azurin with the electrochemical potentials of the substrate (U_S) and ECSTM probe (U_P). The measured height of oxidized azurin ($U_S = 200$ mV) is 0.29 ± 0.01, 0.26 ± 0.005, and 0.22 ± 0.01 nm at ECSTM probe potentials of $U_P = -100$, 150, and 400 mV, respectively ($N = 30$) and can be compared to the height of gold monatomic steps in the same image, which does not change with potentials (0.23 ± 0.01 nm) (see Supporting Information Figure S1). This dependence is in agreement with previous reports[15,23] and is attributed to the redox activity of azurin because this effect is not found in nonredox, Zn-substituted azurin.[23] High apparent heights are obtained when the metal electrode and the redox level of the protein are in resonance conditions.[15]

Electrochemical Current−Distance Spectroscopy. Since the contribution of the redox properties of azurin to the apparent topography of ECSTM images is expected to be complex, we sought a measurement that could be directly correlated to the ET properties of the protein. We thus performed current−distance $I(z)$ tunneling spectroscopy[17,27] of azurin on gold using again ECSTM

under bipotentiostatic control. Semilogarithmic $I(z)$ plots of bare gold and azurin-coated gold are shown in Figure 2a for two initial current set points (3.0 and 0.7 nA) in a 50 mM acetate solution. In bare gold surfaces (blue plots in Figure 2a), an exponential current decay is observed from the initial current set point (3.0 nA) up to the onset of faradaic leakage current of the ECSTM probe away from the surface (50 pA in Figure 2a). This result is according to expectations on a metal surface, and similar curves are obtained at lower set points (not shown). Fitting the exponential region of the plot yields $\beta = 11 \pm 0.1$ nm^{-1} ($N = 10$, $r^2 > 0.99$), in agreement with other studies.[27] This value of β is in the range of the distance decay constants reported for coherent tunneling ET processes observed in a tunneling gap.[27,28] In azurin-coated surfaces (green plots in Figure 2a), the current decays linearly ($r^2 > 0.99$, see inset) at short probe-to-sample distances, and below ~1 nA (corresponding to longer tunneling gap distances), an exponential dependence is again found. Starting from a lower set point (0.7 nA, black plots in Figure 2a), $I(z)$ plots of azurin display a simple exponential decay with $\beta = 4.4 \pm 0.1$ nm^{-1} ($N = 10$). In order to test whether the linear proximity range observed at 3.0 nA set point is related to insufficient surface charge screening,[29] we increased the ionic strength to 1.0 M. In these conditions, the linear range disappears and $I(z)$ plots are exponential even at high current set points (Figure 2b). This result suggests that, at moderate current set points (~1 nA) in 50 mM acetate (low ionic strength), the Debye length (κ^{-1}(nm) = 0.304/$\sqrt{C_{elec}}$(M)) is larger than the STM probe−azurin gap and the probe might penetrate the ionic charge profile over azurin at the imposed set point current (see Supporting Information Figure S3). Thus, the actual electrochemical potential of the probe and azurin is lower than the formal potential applied *versus* the reference electrode in solution; that is, the gap is no longer under potentiostatic control. In this scenario, current decays at a lower than exponential rate with the distance as the tip is retracted from the electrode surface. When the probe−azurin gap is larger than the Debye length, potentiostatic control is recovered. Thus, true potentiostatic control at the tip−sample gap requires current set points in the exponential range.[30]

Electrochemical State Dependence of Distance Decay Constants. Having established suitable conditions for the reliable determination of β, we carried out further $I(z)$ measurements at different U_S and U_P. We initially chose substrate potentials where azurin is reduced (U_S = −300 mV) and oxidized (U_S = 200 mV) and ECSTM probe potentials corresponding to a low, constant bias of 200 mV (U_P = −100 mV and U_P = 400 mV, respectively). After ECSTM imaging bare gold (Figure 3a) and azurin on gold (Figure 3b) at these potentials, we recorded sets of $I(z)$ curves at random locations on each surface. Red traces in Figure 3c,d correspond to

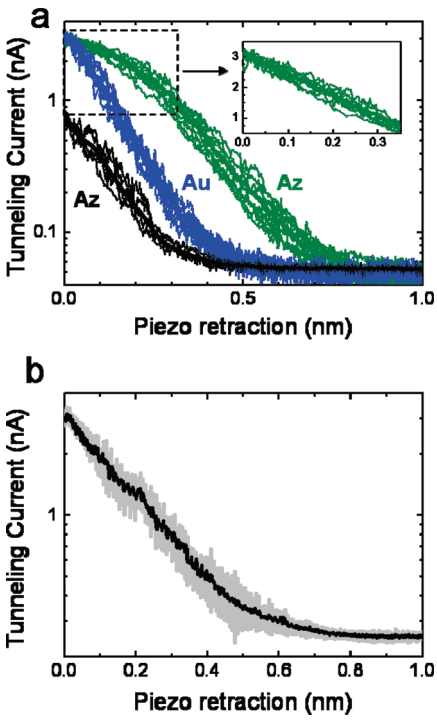

Figure 2. (a) Semilogarithmic current−distance plots of bare gold (in blue) and azurin-coated gold at 3 nA initial set point (in green) and 0.7 nA initial set point (in black), in 50 mM ammonium acetate at U_S = 200 mV, U_P = 400 mV (bias 200 mV). Ten recordings are superimposed in each case to show the experimental variability; averages are indicated using thick traces. Inset: linear-scale zoom of the non-exponential regime at low piezo retraction. (b) Semilogarithmic current−distance plot of azurin-coated gold (3 nA initial set point) in 1.0 M ammonium acetate at U_S = 200 mV, U_P = 400 mV (bias 200 mV). The average and SEM of 10 recordings are indicated in black and gray, respectively.

U_S = −300 mV (reduced azurin) and black traces to U_S = 200 mV (oxidized azurin). In bare gold, $I(z)$ plots are clustered (Figure 3c), and the histogram of β values obtained after individually fitting each plot yields a distribution with a unique maximum centered at 11 nm^{-1} and independent of U_P (Figure 3e). In azurin-coated gold (Figure 3d), two populations of $I(z)$ curves occur with clearly differentiated current decay rates, and the corresponding histograms of β values yield two maxima (Figure 3f). The maximum at 11 nm^{-1} coincides with the value obtained in bare gold and is again independent of U_P. Thus, we interpret that the population of $I(z)$ curves displaying $\beta \approx 11$ nm^{-1} is acquired at bare gold regions on the azurin sample. The maximum of the histogram at $\beta \approx 5$ nm^{-1} does not appear in gold samples and is therefore attributed to azurin. Statistical analysis of the ECTS recordings yields 75% of the curves corresponding to azurin (Figure 3f) and the remaining 25% are similar to curves obtained on bare gold (11 nm^{-1}, Figure 3e). The value of 75% is in agreement with the high azurin coverage observed by ECSTM imaging (Figure3b). The distance decay factor value for azurin is lower than that of bare gold control samples, suggesting a different ET mechanism

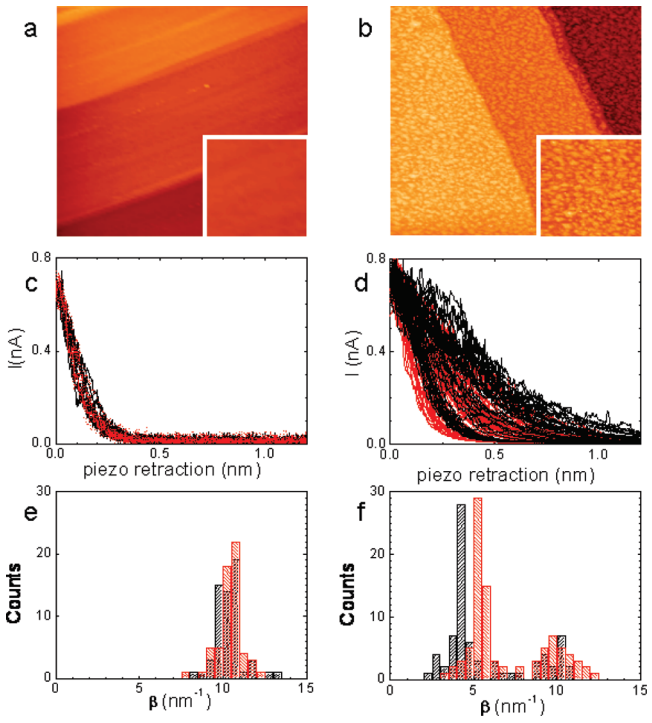

Figure 3. (a) ECSTM image and detail (lower right corner) of a bare gold sample (300 × 300 nm^2 and 80 × 80 nm^2, vertical scale 2 nm). (b) ECSTM image and detail (lower right corner) of an azurin-coated gold sample (300 × 300 nm^2 and 80 × 80 nm^2, vertical scale 2 nm). (c) Ensemble of current−distance plots recorded on bare gold at U_S = 200 mV (black traces) and U_S = −300 mV (red traces) at constant bias of 200 mV. (d) Ensemble of current−distance plots recorded on azurin-coated gold at U_S = 200 mV (black traces, oxidized azurin) and U_S = −300 mV (red traces, reduced azurin) at constant bias of 200 mV. (e) Histogram of the distance decay factor quantified from individual traces in (c). (f) Histogram of the distance decay factor quantified from individual traces in (d).

TABLE 1. Current−Distance Decay Factors (β) of Azurin, Bare Gold and Nonredox Zn-Azurin at Different Sample (U_S) and STM Probe (U_P) Potentials[a]

				β (nm^{-1})		
U_S (V/SSC)	azurin state	U_P (V/SSC)	bias U_P-U_S (V)	azurin	bare gold	Zn-azurin
0.2	oxidized	0.4	0.2	4.4 ± 0.1	11.2 ± 0.3	3.8 ± 0.2
−0.3	reduced	−0.1	0.2	5.4 ± 0.3	10.2 ± 0.2	4.2 ± 0.2
0.2	oxidized	−0.1	−0.3	2.9 ± 0.3	11.7 ± 0.3	4.1 ± 0.2
−0.1	reduced	0.2	0.3	4.5 ± 0.3	10.1 ± 0.2	4.1 ± 0.1

[a] Probe bias is U_P-U_S. Errors indicate standard error of the mean for N = 10 measurements.

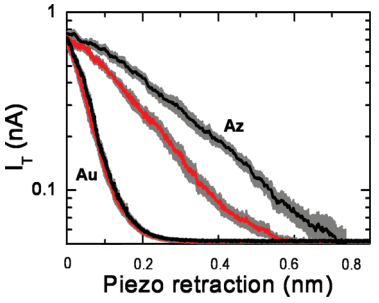

Figure 4. Current−distance plots on bare gold (labeled "Au") averaged from Figure 3c at U_S = 200 mV (black traces) and U_S = −300 mV (red traces) at constant bias of 200 mV. Current−distance plots recorded on azurin-coated gold (labeled "Az"), pooled, and averaged from Figure 3d according to the histogram maxima in Figure 3f. Black traces correspond to U_S = 200 mV (oxidized azurin) and red traces to U_S = −300 mV (reduced azurin) at constant bias of 200 mV.

from a single coherent tunneling step, and it matches the distance decay factor previously predicted for a multistep interprotein ET (5 nm^{-1}, calculated from Figure 5 in ref 11). Interestingly, this maximum occurs at different values under reduced and oxidized conditions (5.4 and 4.4 nm^{-1}, respectively, for a constant bias of 200 mV; see summary in Table 1). In order to find out whether the change in β is due to the redox state of the protein, we measured $I(z)$ curves of nonredox, Zn-substituted azurin as a control experiment (see Supporting Information Figure S2). As shown in Table 1, no significant dependence on potentials was obtained in this case, confirming that the differences found for azurin are due to its redox properties. The $I(z)$ curves of Figure 3d were further pooled according to the histogram maxima (Figure 3f), averaged, and represented in Figure 4 in order to point out differences between the gold substrate, reduced and oxidized azurin.

The exponential dependence found in $I(z)$ plots of azurin (Figure 4) is a signature of tunneling ET mechanism through the protein structure,[31] and the decay

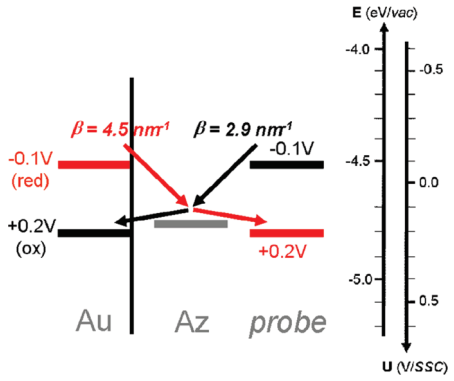

Figure 5. Energy diagram of ET processes in oxidized (U_S = 200 mV, U_P = −100 mV, black arrow) and reduced azurin (U_S = −100 mV, U_P = 200 mV, red arrow). The distance decay constant β corresponding to each ET process is indicated.

constants obtained are in agreement with values mentioned in previous ECSTM studies.[25] Decay constants for ET in azurin have also been obtained from bulk photolysis experiments[7,10] in which redox probes are attached to the protein at different positions and orientations (histidine mutants) in separate experiments; in comparison, each of our $I(z)$ plots provides a direct measurement of β at the single-molecule level and along a well-defined orientation of the protein. We obtain $\beta \approx 5$ nm^{-1} for ET between azurin and the ECSTM probe, a value lower than obtained for intramolecular ET ($\beta \approx 10$ nm^{-1})[7,10,14] but in very good agreement with the distance dependence factor calculated for intermolecular two-step tunneling.[11] Thus, our results confirm multistep tunneling as a mechanism for intermolecular ET involving azurin.

Significant differences in β were obtained between the reduced and oxidized protein, whereas in the cases of Zn-azurin or in the absence of protein, $I(z)$ plots do not change with potential. These results allow for the first time to measure β as a function of the protein redox state and provide access to a wide range of electrochemical potentials of the probe, which is an intrinsic advantage of ECSTM compared to redox probes.[17] In order to test the electrochemical conditions where electrons are injected into oxidized azurin and drawn from its reduced form, we set the potentials at U_S = 200 mV, U_P = −100 mV and U_S = −100 mV, U_P = 200 mV, respectively, which correspond to a moderate, opposite bias of ±300 mV. The values of β obtained for azurin, Zn-azurin, and bare gold are also outlined in Table 1. At these potentials, the decay constants of azurin and gold are again clearly different, and β of the reduced protein (4.5 ± 0.3 nm^{-1}) is also higher than that of the oxidized form (2.9 ± 0.3 nm^{-1}), in agreement with the observations of Figure 3 for bias of 200 mV. The lower values of β found for azurin at ±300 mV bias may be due to the increased bias and to a better overlap of the probe potentials with the azurin redox level. Values of β in control experiments (nonredox protein and bare gold) do not substantially change with potential. These results are depicted in the energy diagram of Figure 5, where the Fermi energies of the gold substrate, ECSTM probe, and the redox level of azurin[23] are represented in the absolute energy scale E(eV) = −e × U(V/SSC) − 4.6 eV.[32,33] When the probe potential is set at U_P = −100 mV, electrons are injected into oxidized azurin (U_S = 200 mV) with a decay constant of 2.9 ± 0.3 nm^{-1} (black arrow in Figure 5), and when U_P = 200 mV, electrons are withdrawn from reduced azurin (U_S = −100 mV) with a decay constant of 4.5 ± 0.3 nm^{-1} (red arrow in Figure 5). The latter situation is formally described as injection of an electron vacancy or "hole". The different β measured in oxidized and reduced azurin indicates an asymmetry in ET with the protein. According to the microreversibility principle, the routes for the corresponding ET reactions should be different. This finding may have implications of biochemical relevance in the respiratory chain and photosynthesis, where azurin is involved in intermolecular ET processes, transporting electrons between partners consisting of membrane proteins. It is well-established that many of the components in the respiratory chains are found in isopotential groups in a near-equilibrium situation,[34] and this defines a process nearly without energy losses. We speculate that, in this context, a protein with redox-dependent β could allow controlling the ET rate or keep unidirectional ET along the chain.

CONCLUSION

We have recorded for the first time current−distance $I(z)$ curves on azurin bound to gold using ECSTM under bipotentiostatic control. We compared azurin to the bare gold surface and to a Zn-substituted azurin as nonredox protein control. The electrochemical potentials of the probe and gold substrate were adjusted independently, and high ionic strength and low initial current set point were required to guarantee good charge screening at the electrodes during the recordings. $I(z)$ curves display an exponential dependence and yield a direct measurement of β, which are characteristic of a two-step tunneling ET process. Significant differences in β between the reduced and oxidized protein were obtained that may be relevant to the control of ET rates in enzymes and biological electron transport chains.

These decay constant measurements are obtained at a well-defined protein orientation, which suggest that by introducing cysteines at different surface locations on azurin and attaching the mutants on an Au/SAM substrate[35] it should be possible to systematically investigate long-range ET along all protein axes, in order to map the preferential ET pathways predicted by simulations. Similarly, mutagenesis should allow studying the role of "redox relay" residues in ET

facilitation.[8] In addition, the method for determination of β can be applied to match the properties of redox partner proteins[12,13] in rationally designed bioelectrochemical nanodevices.

METHODS

Sample Preparation. Reported protocols were used to prepare atomically flat gold surfaces[27] and to attach azurin on gold[25] through native cysteines C3 and C26, which results in a defined orientation of the protein on the surface, while preserving its native-like conformation[36] and electrochemical properties.[23,37] Azurin and all reagents were purchased from Sigma. Nonredox, zinc-substituted azurin for control experiments was obtained as described.[38,39]

Single-Molecule Electrochemical Recordings. ECSTM imaging and spectroscopy experiments were performed with a PicoSPM microscope head and a PicoStat bipotentiostat (Molecular Imaging) controlled by Dulcinea electronics (Nanotec Electrónica). A homemade electrochemical cell was used in four-electrode configuration, using a Pt:Ir (80:20) wire as counter electrode and a miniaturized ultralow leakage membrane Ag/AgCl (SSC) reference electrode filled with 3 M KCl. The potentials of the gold electrode sample (U_S) and ECSTM probe (U_P) are expressed against this reference. Prior to measurements, the electrochemical cell and all of the glass material used for preparation of solutions were cleaned with piranha solution (7:3 H_2SO_4/H_2O_2 (30%) by volume). *Caution: Piranha solution should be handled with extreme caution*. Deionized water (18 MΩ cm^{-1} Milli-Q, Millipore) was used to prepare all solutions and for rinsing samples and electrodes. Unless otherwise specified, the recording solution was 50 mM ammonium acetate buffer at pH 4.55. Pt:Ir ECSTM probes were prepared as described.[24] Data were acquired using WSxM 4.0 software[40] and analyzed with Origin. Current−distance curves were recorded at different U_P and U_S potentials, and an exponential function $I(z) = Ae^{-\beta z}$ was used to fit them ($r^2 \geq 0.99$) in order to obtain the decay factor β. Errors are indicated as standard error of the mean, and N corresponds to the number of measurements.

Acknowledgment. This work was supported in part by Grants PET0808 and CTQ2007-68101-C02 from the Spanish Ministry of Science and Education, and 2009-SGR277 from the Generalitat de Catalunya. I.D.-P. was supported through a MC-IOF within the 7th Framework Programme (European Commission). We also would like to thank C. Vericat, D. Kormes, I. Rimmaudo, C. Rodergas, C. Gómez, and J. Palou for assistance in the experiments, and A. Voityuk, A. Donaire, R. Andreu, M. A. de la Rosa, and J. Hernández-Borrell for discussions.

Supporting Information Available: Azurin apparent height measurements from representative ECSTM images. Current−distance measurements on Zn-azurin. Incomplete charge screening effects affecting current−distance plots at different ionic strengths. This material is available free of charge *via* the Internet at http://pubs.acs.org.

REFERENCES AND NOTES

1. Marcus, R. A.; Sutin, N. Electron Transfers in Chemistry and Biology. *Biochim. Biophys. Acta* **1985,** *811*, 265–322.
2. Hoeben, F. J. M.; Meijer, F. S.; Dekker, C.; Albracht, S. P. J.; Heering, H. A.; Lemay, S. G. Toward Single-Enzyme Molecule Electrochemistry: NiFe-Hydrogenase Protein Film Voltammetry at Nanoelectrodes. *ACS Nano* **2008,** *2*, 2497–2504.
3. Anne, A.; Cambril, E.; Chovin, A.; Demaille, C.; Goyer, C. Electrochemical Atomic Force Microscopy Using a Tip-Attached Redox Mediator for Topographic and Functional Imaging of Nanosystems. *ACS Nano* **2009,** *3*, 2927–2940.
4. Alessandrini, A.; Salerno, M.; Frabboni, S.; Facci, P. Single-Metalloprotein Wet Biotransistor. *Appl. Phys. Lett.* **2005,** *86*, 13902–13905.
5. Tao, N. J. Electron Tansport in Molecular Junctions. *Nat. Nanotechnol.* **2006,** *1*, 173–1816.
6. Bard, A. J. Toward Single Enzyme Molecule Electrochemistry. *ACS Nano* **2008,** *2*, 2437–2440.
7. Langen, R.; Chang, I. J.; Germanas, J. P.; Richards, J. H.; Winkler, J. R.; Gray, H. B. Electron-Tunneling in Proteins—Coupling through a β-Strand. *Science* **1995,** *268*, 1733–1735.
8. Shih, C.; Museth, A. K.; Abrahamsson, M.; Blanco-Rodriguez, A. M.; Di Bilio, A. J.; Sudhamsu, J.; Crane, B. R.; Ronayne, K. L.; Towrie, M.; Vlcek, A.; Richards, J. H.; Winkler, J. R.; Gray, H. B. Tryptophan-Accelerated Electron Flow through Proteins. *Science* **2008,** *320*, 1760–1762.
9. Friis, E. P.; Andersen, J. E. T.; Kharkats, Y. I.; Kuznetsov, A. M.; Nichols, R. J.; Zhang, J. D.; Ulstrup, J. An Approach to Long-Range Electron Transfer Mechanisms in Metalloproteins: *In Situ* Scanning Tunneling Microscopy with Submolecular Resolution. *Proc. Natl. Acad. Sci. U.S.A.* **1999,** *96*, 1379–1384.
10. Gray, H. B.; Winkler, J. R. Electron Tunneling through Proteins. *Q. Rev. Biophys.* **2003,** *36*, 341–372.
11. Gray, H. B.; Winkler, J. R. Long-Range Electron Transfer. *Proc. Natl. Acad. Sci. U.S.A.* **2005,** *102*, 3534–3539.
12. Marshall, N. M.; Garner, D. K.; Wilson, T. D.; Gao, Y.-G.; Robinson, H.; Nilges, M. J.; Lu, Y. Rationally Tuning the Reduction Potential of a Single Cupredoxin beyond the Natural Range. *Nature* **2009,** *462*, 113–116.
13. Lancaster, K. M.; George, S. D.; Yokoyama, K.; Richards, J. H.; Gray, H. B. Type-Zero Copper Proteins. *Nat. Chem.* **2009,** *1*, 711–715.
14. Beratan, D. N.; Betts, J. N.; Onuchic, J. N. Protein Electron-Transfer Rates Set by the Bridging Secondary and Tertiary Structure. *Science* **1991,** *252*, 1285–1288.
15. Chi, Q. J.; Farver, O.; Ulstrup, J. Long-Range Protein Electron Transfer Observed at the Single-Molecule Level: *In Situ* Mapping of Redox-Gated Tunneling Resonance. *Proc. Natl. Acad. Sci. U.S.A.* **2005,** *102*, 16203–16208.
16. Fujita, K.; Nakamura, N.; Ohno, H.; Leigh, B. S.; Niki, K.; Gray, H. B.; Richards, J. H. Mimicking Protein-Protein Electron Transfer: Voltammetry of Pseudomonas Aeruginosa Azurin and the Thermus Thermophilus Cu-A Domain at Omega-Derivatized Self-Assembled-Monolayer Gold Electrodes. *J. Am. Chem. Soc.* **2004,** *126*, 13954–13961.
17. Diez-Perez, I.; Guell, A. G.; Sanz, F.; Gorostiza, P. Conductance Maps by Electrochemical Tunneling Spectroscopy To Fingerprint the Electrode Electronic Structure. *Anal. Chem.* **2006,** *78*, 7325–7329.
18. Monnell, J. D.; Stapleton, J. J.; Dirk, S. M.; Reinerth, W. A.; Tour, J. M.; Allara, D. L.; Weiss, P. S. Relative Conductances of Alkaneselenolate and Alkanethiolate Monolayers on Au{111}. *J. Phys. Chem. B* **2005,** *109*, 20343–20349.
19. Davis, J. J.; Wang, N.; Morgan, A.; Tiantian, Z.; Jianwei, Z. Metalloprotein Tunnel Junctions: Compressional Modulation of Barrier Height and Transport Mechanism. *Faraday Discuss.* **2005,** 167–79.
20. Reed, M. A.; Zhou, C.; Muller, C. J.; Burgin, T. P.; Tour, J. M. Conductance of a Molecular Junction. *Science* **1997,** *278*, 252–254.
21. Xu, B. Q.; Tao, N. J. J. Measurement of Single-Molecule Resistance by Repeated Formation of Molecular Junctions. *Science* **2003,** *301*, 1221–1223.
22. Tao, N. J. Probing Potential-Tuned Resonant Tunneling through Redox Molecules with Scanning Tunneling Microscopy. *Phys. Rev. Lett.* **1996,** *76*, 4066–4069.
23. Alessandrini, A.; Corni, S.; Facci, P. Unravelling Single Metalloprotein Electron Transfer by Scanning Probe Techniques. *Phys. Chem. Chem. Phys.* **2006,** *8*, 4383–4397.

24. Guell, A. G.; Diez-Perez, I.; Gorostiza, P.; Sanz, F. Preparation of Reliable Probes for Electrochemical Tunneling Spectroscopy. *Anal. Chem.* **2004,** *76*, 5218–5222.
25. Friis, E. P.; Andersen, J. E. T.; Madsen, L. L.; Moller, P.; Ulstrup, J. *In Situ* STM and AFM of the Copper Protein *Pseudomonas aeruginosa* Azurin. *J. Electroanal. Chem.* **1997,** *431*, 35–38.
26. Gray, H. B.; Winkler, J. R. Electron Flow through Proteins. *Chem. Phys. Lett.* **2009,** *483*, 1–9.
27. Nagy, G.; Wandlowski, T. Double Layer Properties of Au(111)/H_2SO_4 (Cl)+Cu^{2+} from Distance Tunneling Spectroscopy. *Langmuir* **2003,** *19*, 10271–10280.
28. Li, X. L.; He, J.; Hihath, J.; Xu, B. Q.; Lindsay, S. M.; Tao, N. J. Conductance of Single Alkanedithiols: Conduction Mechanism and Effect of Molecule−Electrode Contacts. *J. Am. Chem. Soc.* **2006,** *128*, 2135–2141.
29. Wigginton, N. S.; Rosso, K. M.; Stack, A. G.; Hochella, M. F. Long-Range Electron Transfer across Cytochrome-Hematite (α-Fe_2O_3) Interfaces. *J. Phys. Chem. C* **2009,** *113*, 2096–2103.
30. Although this can be accomplished at 3 nA in 1.0 M solution, such high ionic strength also causes high probe leakage due to increased solution conductivity and wear of the insulating films as a result of excessive charging (note the 0.3 nA leakage in Figure 1b). A tradeoff was thus required, and in all subsequent experiments, we opted by using the nearly physiological 50 mM solution employed in previous studies[4,9] and a 0.7 nA set point, which lies within the exponential decay range while leaving a ~3 Å z-retraction window for most insulated probes (~50 pA leak).
31. McCreery, R. L. Molecular Electronic Junctions. *Chem. Mater.* **2004,** *16*, 4477–4496.
32. Morrison, S. R. *Electrochemistry at Semiconductor and Oxidized Metal Electrodes*; Plenum Press: New York, 1980.
33. Gerischer, H.; Ekardt, W. Fermi Levels in Electrolytes and the Absolute Scale of Redox Potentials. *Appl. Phys. Lett.* **1983,** 393–395.
34. Wilson, D. F.; Stubbs, M.; Veech, R. L.; Erecinsk., M; Krebs, H. A. Equilibrium Relations between Oxidation−Reduction Reactions and Adenosine-Triphosphate Synthesis in Suspensions of Isolated Liver-Cells. *Biochem. J.* **1974,** *140*, 57–64.
35. Machczynski, M. C.; Kuhl, K. P.; McGuirl, M. A. Modulation of the Electrochemical Behavior of Tyrosyl Radicals by the Electrode Surface. *Anal. Biochem.* **2007,** *362*, 89–97.
36. Pompa, P. P.; Bramanti, A.; Maruccio, G.; Cingolani, R.; De Rienzo, F.; Corni, S.; Di Felice, R.; Rinaldi, R. Retention of Nativelike Conformation by Proteins Embedded in High External Electric Fields. *J. Chem. Phys.* **2005,** *122*, 181102–181106.
37. Chi, Q. J.; Zhang, J. D.; Friis, E. P.; Andersen, J. E. T.; Ulstrup, J. Electrochemistry of Self-Assembled Monolayers of the Blue Copper Protein *Pseudomonas aeruginosa* Azurin on Au(111). *Electrochem. Commun.* **1999,** *1*, 91–96.
38. Fuentes, L.; Oyola, J.; Fernandez, M.; Quinones, E. Conformational Changes in Azurin from *Pseudomona aeruginosa* Induced through Chemical and Physical Protocols. *Biophys. J.* **2004,** *87*, 1873–1880.
39. Miller, J. E. Radical Formation and Electron Transfer in Biological Molecules. Ph.D. Dissertation, California Institute of Technology, 2004.
40. Horcas, I.; Fernandez, R.; Gomez-Rodriguez, J. M.; Colchero, J.; Gomez-Herrero, J.; Baro, A. M. *Rev. Sci. Instrum.* **2007,** *78*, 13705–13713.